


Spin transport from order to disorder

Derek Reitz  and Yaroslav Tserkovnyak

Department of Physics and Astronomy and Bhaumik Institute for Theoretical Physics, University of California, Los Angeles, California 90095, USA

 (Received 7 July 2023; accepted 21 September 2023; published 16 October 2023)

Schwinger boson mean-field theory (SBMFT) is a nonperturbative approach which treats ordered and disordered phases of magnetic systems on equal footing. We leverage its versatility to evaluate the spin correlators which determine thermally induced spin transport the spin Seebeck effect (SSE) in Heisenberg ferromagnets (FMs) and antiferromagnets (AFMs), at arbitrary temperatures. In SBMFT, the spin current J_s is made up of particle-hole-like excitations which carry integral spin angular momentum. Well below the ordering temperature, J_s is dominated by a magnonic contribution, reproducing the behavior of a dilute-magnon gas. Near the transition temperature, an additional, paramagneticlike contribution becomes significant. In the AFM, the two contributions come with opposite signs, resulting in a signature, rapid inversion of the spin Seebeck coefficient as a function of temperature. Ultimately, at high temperatures, the low-field behavior of the paramagnetic SSE reduces to Curie-Weiss physics. An analysis based on our theory confirms that in recent experiments on gadolinium gallium garnet, the low-field spin Seebeck coefficient $S(T) \propto \chi(T)$, the spin susceptibility, down to the Curie-Weiss temperature. At lower temperatures in the disordered phase, our theory shows a deviation of $S(T)$ relative to $\chi(T)$ in both FMs and AFMs, which increases with decreasing temperature and arises due to a paramagnetic liquid phase in our theory. These results demonstrate that the SSE can be a probe of the short-ranged magnetic correlations in disordered correlated spin systems and spin liquids.

DOI: [10.1103/PhysRevB.108.L140407](https://doi.org/10.1103/PhysRevB.108.L140407)

Introduction. Most works in spintronics based on magnetic systems are asymptotic expansions or tailored phenomenological models which can be loosely divided into three categories: the strongly ordered regime that is handled by the Holstein-Primakoff approximation (HPA) and related treatments in three dimensions (3D), the nonlinear- σ model, or the Landau-Lifshitz-Gilbert phenomenology; the completely disordered paramagnetic Curie-Weiss regime; or criticality described by Landau theory. While the associated theories may work well in their respective small-parameter regimes, they fail outside of them. Moreover, phenomenology must be supported by an underlying fundamental description which contains the basic physical ingredients. The Schwinger boson transformation takes $SU(\mathcal{N})$ generators to a product of \mathcal{N} bosonic operators. The Hamiltonian is then decoupled by a Hubbard-Stratonovich transformation where the mean-field theory is the saddle point (SP), and the order n fluctuations about the SP scale as $O(1/\mathcal{N}^n)$ [1,2]. This approach, on the other hand, has no small or large parameter for fixed $\mathcal{N} \sim 1$, but still has the ability to qualitatively capture essential physics in regimes where we do not have an accurate theory.

The spin Seebeck effect (SSE) is generated by thermalized spin excitations and requires broken symmetry in spin space. Starting at $T \ll T_{C(N)}$, the Curie (Néel) temperatures, in ordered magnets, spin Seebeck coefficients theoretically [3–8] and experimentally [9–11] are generally expected to be enhanced by increasing temperature, while the opposite holds for paramagnets [12–17], with the largest signals near the transition temperatures [4,14,18,19]. These results suggest that the optimal regimes for thermoelectric applications may be distinct from the ones best described by HPA or the

Curie-Weiss law, for example, which are designed to incorporate disorder or order, respectively, as minor corrections. In Schwinger boson mean-field theory (SBMFT), the ferromagnetic (FM), antiferromagnetic (AFM), and paramagnetic (PM) spin Seebeck coefficients reach their maxima around $T_{C(N)}$, where they reach the same order of magnitude when the Zeeman energy $\hbar\gamma B \approx J$, the exchange constant. While the SBMFT spin Seebeck coefficients in FMs and PMs have the same sign, in AFMs the SSE inverts in sign slightly below T_N due to the competition between antiferromagnetic and paramagnetic fluctuations.

The liquid-gas crossover in Heisenberg FMs and AFMs appears as a continuous transition in SBMFT, and occurs at their Curie-Weiss temperatures Θ_{CW} , with frustration parameter $f \equiv |\Theta_{CW}|/T_{C(N)} \gtrsim 1$ in 3D. The liquid phase of the Heisenberg model in SBMFT is a simple setting for studying correlations effects in disordered spin systems, in 3D, as shown here, and also 2D [20–24]. For example, by evaluating the spin correlators involved in thermally induced spin transport across the paramagnetic phase, we show how spin Seebeck experiments can probe the properties of interacting spin liquids. SBMFT may play an important role for understanding spin transport measurements that can be used to manifest the magnetic properties of spin liquids [25,26]. This would complement indirect measurements such as the thermal conductivity and can support the limited information extracted from NMR and magnetic susceptibility measurements [27]. Along these lines, we introduce the parameter $p(T) \equiv \partial_B S/\chi$, the ratio of the SSE to the spin susceptibility, which is T independent when a magnet is completely disordered and becomes T dependent when short-ranged spin correlations are

significant to spin transport. $p(T)$ is then an indicator for spin correlations in the paramagnetic regime.

Mean-field theory. The Schwinger boson transformation replaces the spin operators by a product of bosonic creation and annihilation operators, $S^+ = a_\uparrow^\dagger a_\downarrow$, $S^- = a_\downarrow^\dagger a_\uparrow$, $S^z = \sum_\sigma \sigma a_\sigma^\dagger a_\sigma / 2$, with the spin length fixed on each site by the constraint $S = \sum_\sigma a_\sigma^\dagger a_\sigma / 2$. The SU(2)-preserving mean-field decomposition of the nearest-neighbor Heisenberg Hamiltonian on a bipartite lattice, written in terms of Schwinger bosons (SBs) a_σ and b_σ for sublattices \mathcal{A} and \mathcal{B} , respectively, is

$$H_{\text{mf}}^{\text{SU}(2)} = -2J \sum_{\langle ij \rangle} [\alpha F_{ij}^\dagger F - (1 - \alpha) A_{ij}^\dagger A] + \text{H.c.} \\ - \mu_{\mathcal{A}} \sum_{i \in \mathcal{A}, \sigma} a_{i\sigma}^\dagger a_{i\sigma} - \mu_{\mathcal{B}} \sum_{i \in \mathcal{B}, \sigma} b_{i\sigma}^\dagger b_{i\sigma}. \quad (1a)$$

Here, summing over $\langle ij \rangle$ avoids double counting, $F_{ij} = \sum_\sigma a_{i\sigma}^\dagger b_{j\sigma} / 2$ is a ‘‘ferromagnetic’’ contribution, and $A_{ij} = \sum_\sigma \sigma a_{i\sigma} b_{j\sigma} / 2$ is an ‘‘antiferromagnetic’’ contribution [28].

These quartic terms are approximated in our mean-field (MF) decomposition by the product of a quadratic term and the mean fields $F = \langle F_{ij} \rangle$ and $A = \langle A_{ij} \rangle$, and in the same spirit the spin length constraints are implemented via two aggregate Lagrange multipliers $\mu_{\mathcal{A}(\mathcal{B})}$. This decomposition applies to isotropic lattice models where there is a single F and single A parameter. Note that while the exact constraint fixes the sum of the SB species’ number operators on each site, $\mu_{\mathcal{A}(\mathcal{B})}$ instead fix the expectation value of this operator sum on each sublattice. α is a parameter that is free to vary in the exact Hamiltonian, but parametrizes separate mean-field Hamiltonians [2,28]. To fix α , we match the poles of the dynamic susceptibilities to the Holstein-Primakoff result at $T = 0$, giving the usual [1] $\alpha = 1$ for the FM and $\alpha = 0$ for the AFM, and for simplicity fix these values for α at all T . In total, the bipartite FM (uniaxial AFM below spin flop) has three mean-field parameters: F (A), $\mu \equiv (\mu_{\mathcal{A}} + \mu_{\mathcal{B}})/2$, and $\delta\mu \equiv (\mu_{\mathcal{A}} - \mu_{\mathcal{B}})/2$. For the most general (Hartree-Fock-Bogoliubov) U(1)-preserving mean-field decomposition, see the Supplemental Material (SM) [29].

When $T \ll T_{C(N)}$, thermal equilibrium described by the Holstein-Primakoff picture is characterized by a dilute magnon gas with a single band for each sublattice [30], which slightly depolarizes the spin ordering. In SBMFT, there are twice as many bands as in HPA, and each SB band carries half-integer spin. At a glance, the two pictures may seem irreconcilable. However, at T_C in FMs the lowest-energy modes of one SB spin species (in the axially symmetric case, for example) reach zero energy and form a Bose-Einstein condensate, resulting in long-ranged ordering along that species’ spin polarization. At T_N in AFMs, long-ranged staggering ordering arises from condensation of one spin species on sublattice \mathcal{A} , and the opposite spin species on sublattice \mathcal{B} . Magnons in SBMFT are then spinful excitations associated with transitions from the condensates to the thermal cloud, as shown in Fig. 1. Thus, the SB bands on each sublattice which carry spin opposite to the local order mimic the magnon bands in Holstein-Primakoff. As we will see, these magnonic excitations will dominate spin transport at $T \ll T_{C(N)}$.

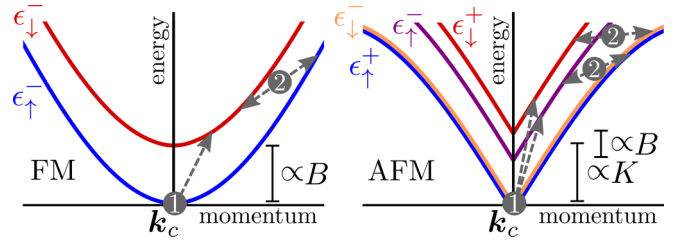


FIG. 1. Schematic depiction of the magnonic (1) and paramagnetic-like (2) contributions to J_s . Each color specifies a combination of the bands’ lower-indexed spin polarization and upper-indexed pseudospin. In SBMFT for FMs (AFMs), at $T \leq T_{C(N)}$, Bose-Einstein condensation occurs at the lowest-energy modes with momentum \mathbf{k}_c . At $T > T_{C(N)}$ a self-consistent gap $-\mu$ opens up.

The SU(2)-preserving mean-field theory (MFT) yields a first-order Curie transition on cubic Bravais lattices, but is second order on the diamond lattice, possibly due to its higher-order connectivity [31]. The FM mean-field Hamiltonian plus applied field on the diamond lattice, setting $\delta\mu = 0$, after Fourier transforming and casting in terms of sublattice pseudospin, $\psi_{\mathbf{k}\sigma} = (a_{\mathbf{k}\sigma}, b_{\mathbf{k}\sigma})$, is

$$H_{\text{mf}}^{\text{FM}} = \sum_{\mathbf{k}\sigma} \psi_{\mathbf{k}\sigma}^\dagger [-(\mu + b\sigma/2) + \boldsymbol{\eta}_{\mathbf{k}} \cdot \boldsymbol{\tau}] \psi_{\mathbf{k}\sigma}, \quad (2)$$

where $b \equiv \hbar\gamma B$, $\boldsymbol{\eta}_{\mathbf{k}} = JF(-\text{Re } \gamma_{\mathbf{k}}, \text{Im } \gamma_{\mathbf{k}}, 0)$, $\gamma_{\mathbf{k}} = Z^{-1} \sum_{\delta} e^{i\mathbf{k} \cdot \delta}$ is the structure factor, δ is the vector between nearest neighbors on sublattice \mathcal{A} to \mathcal{B} , and $\boldsymbol{\tau}$ is the vector of Pauli matrices. There are four bands with energies

$$\epsilon_{\mathbf{k}\sigma}^{\pm} = JZF(1 \pm |\gamma_{\mathbf{k}}|) - (\mu + b\sigma/2), \quad (3)$$

where a factor of JZF was absorbed into the definition of μ . The eigenvectors are $v_{\mathbf{k}\sigma}^{\pm} = (1, \mp |\gamma_{\mathbf{k}}|/\gamma_{\mathbf{k}})/\sqrt{2}$. If μ reaches $-b/2$, the lowest-energy branch $\epsilon_{\mathbf{k}\uparrow}^-$ has zero-energy modes that condense, resulting in long-ranged spin ordering along the $+\hat{z}$ axis in the language of SBs [1,32]. The lower-energy ϵ^- bands are shown in Fig. 1, and shown along with the high-energy ϵ^+ bands in Supplemental Material Fig. 3 [29]. At arbitrary temperatures, the self-consistent mean-field equations for F and S give the solutions to $F(T)$ and either the condensate density $n_c(T)$ or $\mu(T)$ according to

$$F = -(4N)^{-1} \sum_{\mathbf{k}\sigma\lambda} n_{\mathbf{k}\sigma\lambda}^\lambda \lambda |\gamma_{\mathbf{k}}|, \quad S = (4N)^{-1} \sum_{\mathbf{k}\sigma\lambda} n_{\mathbf{k}\sigma\lambda}^\lambda, \quad (4)$$

where $n_{\mathbf{k}\sigma}^\lambda$ is the Bose-Einstein distribution function for energy $\epsilon_{\mathbf{k}\sigma}^\lambda$, and N is the number of sites per sublattice. In order to solve Eqs. (4) at $T < T_C$, the sums are converted to integrals with the contributions from the condensate density separated explicitly: For an arbitrary function z and a single condensation point at momentum \mathbf{k}_c , $\sum_{\mathbf{k}} z_{\mathbf{k}}/N \approx z(\mathbf{k}_c)n_c + \mathcal{V} \int_{\text{BZ}} d^3\mathbf{k} z(\mathbf{k})/(2\pi)^3$, where $n_c \equiv N_c/N$ and \mathcal{V} is the unit cell volume.

On the other hand, we find the Néel transition is second order on all cubic Bravais lattices, so we take the simple cubic lattice for simplicity. The AFM mean-field Hamiltonian with easy-axis anisotropy constant K plus collinear applied

field is

$$H_{\text{mf}}^{\text{AFM}} = \sum_{k\sigma} \psi_{k\sigma}^\dagger [\zeta_\sigma - (\delta\mu + b\sigma/2)\tau_z] \psi_{k\sigma} + \sum_{k\sigma} (i\sigma \psi_{k\sigma}^\dagger \boldsymbol{\eta}_k \cdot \boldsymbol{\tau} \psi_{-k\bar{\sigma}}/2 + \text{H.c.}), \quad (5)$$

where we consider $b \ll \sqrt{JK}$, the spin-flop field; here, $\zeta_\sigma = -\mu - KL^z\sigma/2$ for mean staggered spin polarization $L^z = (S_A^z - S_B^z)/2$, $\boldsymbol{\eta}_k = JA(\text{Im } \gamma_k, \text{Re } \gamma_k, 0)$, and ψ^\dagger is the vector transpose. Diagonalizing the Hamiltonian via a Bogoliubov transformation for each σ yields four bands (see SM [29]), so we get energies

$$\begin{aligned} \epsilon_{k\sigma}^+ &= -\delta\mu - b\sigma/2 + \epsilon_{k\sigma}, & \epsilon_{k\sigma}^- &= \delta\mu - b\sigma/2 + \epsilon_{k\bar{\sigma}}, \\ \epsilon_{k\sigma} &\equiv \sqrt{\zeta_\sigma(2JZA + \zeta_\sigma) + (JZA)^2(1 - \gamma_k^2)}, \end{aligned} \quad (6)$$

where, as for the FM, we shifted μ by a factor of JZA , and $\bar{\sigma} = -\sigma$. Here, the ansatz $\delta\mu = -b/2$ was found by matching the field splitting of $\epsilon_{k\downarrow}^+$ and $\epsilon_{k\uparrow}^-$ to that of the usual AFM magnon modes from HPA. This is a self-consistent solution for $T < T_N$, and then $\delta\mu = 0$ for $T \geq T_N$. Analogously to the FM, BEC occurs when the lowest-energy modes of $\epsilon_{k\uparrow}^+$ and $\epsilon_{k\downarrow}^-$ become gapless at $\mu = -KL^z/2$, so that $\zeta_\sigma = KL^z(1 - \sigma)/2$ [33], resulting in long-ranged staggered ordering. The modes are depicted in Fig. 1. The equations for $T < T_N$ are obtained by eliminating $n_c(T)$ to give two independent equations for $A(T)$ and $L^z(T)$, which in the limit $K \ll J$ (e.g., in Cr_2O_3 , $K \approx 7 \times 10^{-2}J$ [34]) are

$$A = S + C^A - (4N)^{-1} \sum_{k\sigma} (n_{k\sigma}^+ + n_{k\bar{\sigma}}^-) \sqrt{1 - \gamma_k^2}, \quad (7a)$$

$$L^z = S - C^z - (2N)^{-1} \sum_k (n_{k\downarrow}^+ + n_{k\uparrow}^-) / \sqrt{1 - \gamma_k^2}, \quad (7b)$$

where $C_A = 1/2 - (2N)^{-1} \sum_k \sqrt{1 - \gamma_k^2} \approx 0.13$, $C_z = 1/2 - (N)^{-1} \sum_k 1/\sqrt{1 - \gamma_k^2} \approx 0.25$, the contributions from the zero-energy modes vanish in Eq. (7a), and Eq. (7b) only contains finite-energy modes. At $T > T_N$, $L^z = 0$ and $\mu(T)$ is no longer fixed so the mean-field equations are

$$A = (2N)^{-1} \sum_{k\sigma} (n_{k\sigma} + 1/2) \sqrt{(-\mu + JZA)^2 / \epsilon_{k\sigma}^2 - 1}, \quad (8a)$$

$$S = -1/2 + (2N)^{-1} \sum_{k\sigma} (n_{k\sigma} + 1/2) (-\mu + JZA) / \epsilon_{k\sigma}, \quad (8b)$$

where we took $n_{k\sigma}^+ \approx n_{k\sigma}^- \equiv n_{k\sigma}$ (valid when $K \ll J$).

Finally, we compare the SBMFT magnonic excitations to the HPA dispersions in the strongly ordered phases. In the diamond-lattice FM, the lowest-energy modes of the $\epsilon_{k\uparrow}^-$ band condense and the two $\epsilon_{k\downarrow}^\pm$ bands match the magnon bands from HPA, which reproduces the usual Bloch $T^{3/2}$ law for demagnetization at $T \ll T_C$ [35]. In the simple-cubic-lattice AFM, the lowest-energy modes of the $\epsilon_{k\uparrow}^+$ and $\epsilon_{k\downarrow}^-$ bands condense at T_N forming staggered ordering while the $\epsilon_{k\downarrow}^+$ and $\epsilon_{k\uparrow}^-$ bands qualitatively match the magnon bands from HPA. They are $\epsilon_{k\downarrow}^+, \epsilon_{k\uparrow}^- = \pm b + \epsilon_k$, where $\epsilon_k = \sqrt{\epsilon_0^2 + (JZA)^2(1 - \gamma_k^2)}$

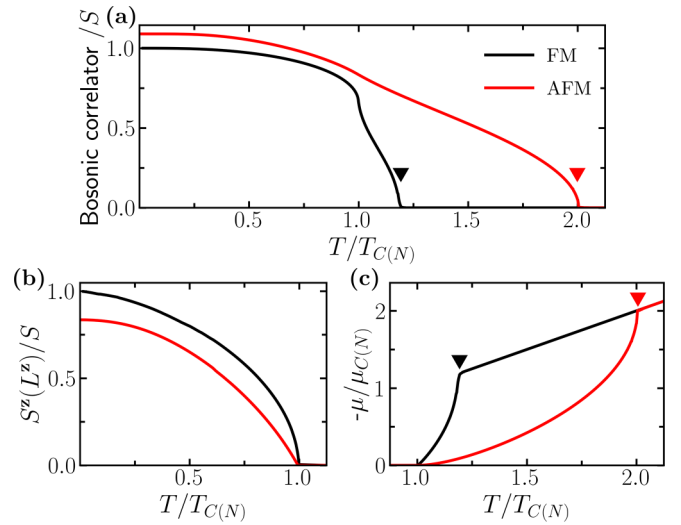


FIG. 2. Mean-field solutions for the $S = 1/2$ FM on the diamond lattice and the $S = 3/2$ AFM on the simple cubic lattice. For the FM (AFM), (a) shows F (A), (b) shows S^z (L^z), and (c) shows $-\mu$ in units of $\mu_{C(N)} = -T_{C(N)} \ln(1/S + 1)$. Triangular markers denote the positions of the liquid-gas crossover.

with $\epsilon_0^2 = \epsilon_K(\epsilon_K + 2JZA)$ and $\epsilon_K = KL^z$. At $T \ll T_N$, the dispersive term $(JZA)^2(1 - \gamma_k^2)$ with $A/S = 1 + C_A/S$ differs by a constant factor from the HPA value, and the gap ϵ_0 is proportional to $\epsilon_K = K(S - 1/2)$ in HPA while it is $\epsilon_K = K(S - 1/2 + C_z)$ in SBMFT. The complete numerical solutions of the MFT for $B = 0$ with $S = 1/2$ for the FM, where $n_c \propto S^z$, and $S = 3/2$ for the AFM, where $n_c \propto L^z$, are plotted in Fig. 2 ($T_C = 0.633J$ and $T_N = 5.12J$ in units where the Boltzmann constant $k_B = 1$).

Spin transport. The net interfacial spin current between a magnetic insulator at T_1 and a metal at T_2 may be computed by treating the interfacial exchange Hamiltonian perturbatively with respect to the bulk. If we consider a ferromagnetic Bravais lattice with interfacial Hamiltonian in momentum space $H_{\text{int}} = (V/N) \sum_{k,k',q,q'} a_{k\uparrow}^\dagger a_{k'\downarrow} c_{q\downarrow}^\dagger c_{q'\uparrow} + \text{H.c.}$, we get via Fermi's golden rule (FGR) for the interfacial spin current density (in units of energy per area),

$$J_s = \frac{g_{\uparrow\downarrow}}{2SN^2} \sum_{k,k'} \epsilon_{kk'\uparrow\downarrow} [n_1(\epsilon_{k\uparrow}) - n_1(\epsilon_{k'\downarrow}) \times [n_1(\epsilon_{kk'\uparrow\downarrow}) - n_2(\epsilon_{kk'\uparrow\downarrow})], \quad (9)$$

where $\epsilon_{kk'\uparrow\downarrow} \equiv \epsilon_{k\uparrow} - \epsilon_{k'\downarrow}$, and $g_{\uparrow\downarrow} \equiv 4\pi SD^2 V^2 / \mathcal{A}$ [36] is in units of inverse area where D is the metal's density of states at the Fermi level in units of $(\text{energy} \cdot \text{volume})^{-1}$ and \mathcal{A} is the area per site of the interface. Equation (9) shows that J_s is made up of particle-hole-like excitations which carry spin angular momentum. In the bipartite FM and AFMs, the SBs on each sublattice split into mixtures of the two pseudospin SBs (for the full expressions for J_s there, see the Supplemental Material [29]). Finally, the spin Seebeck coefficient for $J_s(T_1, T_2)$ is defined as $\mathcal{S}(T) \equiv J_s(T + \delta T, T - \delta T) / \delta T$ in the limit $\delta T \ll T$ of linear response.

In the ordered phases, the condensates grow macroscopically large. In the thermodynamic limit, they must be separated from the integrals over the BZ. The contribution to the FM spin Seebeck coefficient on diamond due to the

condensate density $n_c \propto S^z$ is

$$\mathcal{S}^{\text{FM}} = \frac{g_{\uparrow\downarrow}}{2s} S^z \int \frac{d^3\mathbf{k}}{(2\pi)^3} \partial_T (\epsilon_{k\downarrow}^+ n_{k\downarrow}^+ + \epsilon_{k\downarrow}^- n_{k\downarrow}^-), \quad (10)$$

where $s \equiv S/\mathcal{V}$, and $\epsilon_{k\downarrow}^\pm$ are the magnon energies. For the AFM, we consider an interface which is compensated in aggregate but comprises separate islands where the metal couples directly to either one of the two sublattices, and negligibly to the other [7,37]. In this scenario, the AFM spin current is $J_s = J_s^A + J_s^B$, where J_s^A is generated by the coupling $H_{\text{int}}^A = (V/N) \sum_{\mathbf{k}, \mathbf{k}', q, q'} a_{\mathbf{k}\uparrow}^\dagger a_{\mathbf{k}'\downarrow} c_{q\downarrow}^\dagger c_{q'\uparrow} + \text{H.c.}$ and J_s^B by $H_{\text{int}}^B = (V/N) \sum_{\mathbf{k}, \mathbf{k}', q, q'} b_{\mathbf{k}\uparrow}^\dagger b_{\mathbf{k}'\downarrow} c_{q\downarrow}^\dagger c_{q'\uparrow} + \text{H.c.}$. The contribution to the AFM spin Seebeck coefficient due to the condensate density $n_c \propto L^z$ is

$$\mathcal{S}^{\text{AFM}} = \frac{g_{\uparrow\downarrow}}{2s} L^z \int \frac{d^3\mathbf{k}}{(2\pi)^3} \frac{2JZA}{\epsilon_{k\downarrow}^+ + \epsilon_{k\uparrow}^-} \partial_T (\epsilon_{k\downarrow}^+ n_{k\downarrow}^+ - \epsilon_{k\uparrow}^- n_{k\uparrow}^-). \quad (11)$$

The AFM SSE has contributions at the two magnon energies, $\epsilon_{k\downarrow}^+$ and $\epsilon_{k\uparrow}^-$, which come with opposite signs since they carry oppositely oriented spin angular momentum. Equation (11) at $T \ll T_N$ reproduces the semiclassical Néel spin current derived in Ref. [8].

At larger temperatures, J_s also contains a contribution from scattering between bands in the thermal cloud, as shown in Fig. 1. This contribution is relatively smaller at $T \ll T_{C(N)}$ and becomes the paramagnetic spin current at $T > T_{C(N)}$. In order to carry out the two sets of integrals numerically in \mathcal{S}^{PM} , we approximate the band structure with the low-energy, long-wavelength dispersion: $\epsilon_{k\sigma}^\pm \approx JFk^2 - (\mu + b\sigma/2)$ for the FM and $\epsilon_{k\sigma}^\pm \approx \pm(1 - \sigma)b/2 + \sqrt{\zeta_\sigma^2 - 2Z(JAk)^2}$ for the AFM. The SBMFT spin Seebeck coefficients are compared to those computed in the same fashion using the Holstein-Primakoff transformation [36]. The Holstein-Primakoff result is obtained by Taylor expanding the transformed spin operators to first order in $1/S$, denoted as the Holstein-Primakoff approximation (HPA). In the HPA, the Heisenberg Hamiltonian is quartic in the magnon field operators, but we approximate it by a Hartree-Fock mean-field decomposition which contains only quadratic terms. The magnon correlators in the spin current are then reduced to quadratic correlators via Wick's theorem. The results are plotted as a function of temperature in Fig. 3.

In strongly disordered spin systems, spin correlations decay on the scale of the lattice spacing. In SBMFT, this corresponds to $JF, JA \ll T$, and is described by the gaseous phase of the theory. In the gaseous phase at $b \ll T$, we get $\partial_B \mathcal{S}^{\text{PM}} = \chi g_{\uparrow\downarrow}$ where $\chi \equiv \partial_B S^z / S$ is the normalized spin susceptibility. As T decreases below Θ_{CW} in the SBMFT, this treatment has a continuous liquid-gas phase transition and spin correlations start to become significant. When JF or $JA \sim T$, $\partial_B \mathcal{S}^{\text{PM}}$ deviates from χ . Based on this analysis of the Heisenberg model in SBMFT, we introduce a new parameter $p(T) \equiv \partial_B \mathcal{S} / \chi$, whose temperature dependence is an indicator for short-ranged spin correlations as shown in Fig. 4 (for comparison purposes, χ is also computed in the same fashion as \mathcal{S}^{PM} discussed above).

Discussion. Experimentally, extracting $p(T) \equiv \partial_B \mathcal{S} / \chi$ (Fig. 4) is complicated since the measured spin Seebeck voltage, $V(B, T) = \mathcal{S}(B, T)f(T)$, contains additional

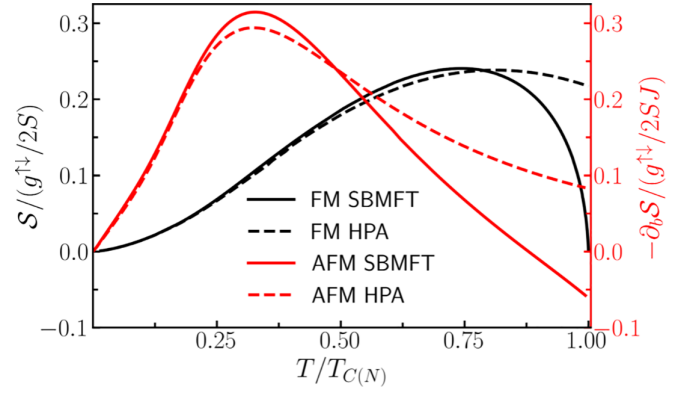


FIG. 3. The spin Seebeck coefficients for the $S = 1/2$ FM on the diamond lattice and the negative field derivative $-\partial_b \mathcal{S}$ (with $b = \hbar\gamma B$) for the $S = 3/2$ AFM on the simple cubic lattice computed in the limit $B \rightarrow 0$ using SBMFT and HPA.

temperature-dependent factors in $f(T)$, such as the interfacial thermal conductivity and metallic resistivity [8,17]. However, we can analyze how the magnetic field profile, of the measured $V(B, T)$ and theoretical $\mathcal{S}(B, T)$, evolve with temperature. We illustrate this by comparing our theory for the SSE at $T \gg T_{C(N)}$ to experiments in gadolinium gallium garnet (GGG) [13,14]. This approach involves comparing salient features in the magnetic field dependence at separate temperatures, such as the slope at low fields [8]. Here, we identify the field position of the peak in the SSE as a quantity which contains information about $\mathcal{S}(B, T)$, but is independent of $f(T)$. The peak data points are extracted from SSE field sweeps, and our theoretical values rely solely on the magnet's Curie-Weiss temperature. When we use an independently measured value for Θ_{CW} from the static susceptibility in GGG [38], we find that our theory quantitatively reproduces the experimental SSE peak positions down to $T \geq 2 \text{ K} \approx \Theta_{\text{CW}}$, as shown in Fig. 5 (these are the lowest-temperature data currently available; for the complete field dependencies, see the

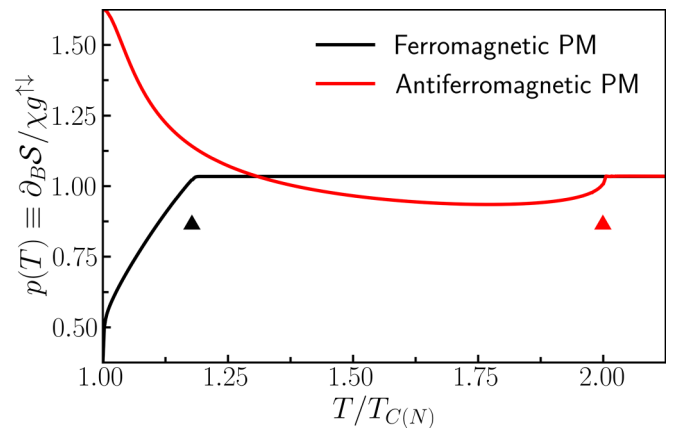


FIG. 4. Field derivative of the paramagnetic SSE relative to the spin susceptibility in FMs and AFMs. Coming from above along the temperature axis, $\partial_B \mathcal{S} / g_{\uparrow\downarrow}$ begins to deviate from χ at the liquid-gas crossovers denoted by triangular markers.

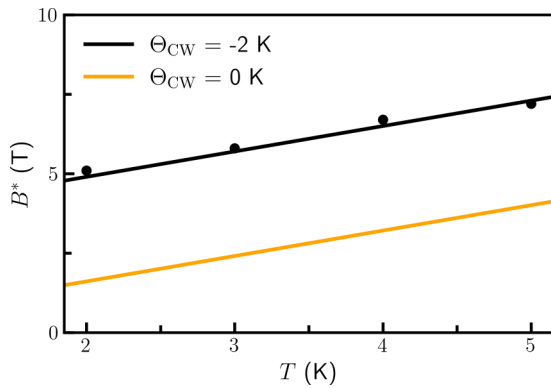


FIG. 5. The magnetic field where the SSE is maximized is plotted (data plotted as solid circles at $T = 2, 3, 4$ K from Ref. [14] and $T = 5$ K from Ref. [13]), which depends only on the spin Seebeck coefficient. The theory contains a single, constant undetermined parameter: the Curie-Weiss temperature Θ_{CW} , after we took $S = 7/2$ for GGG.

Supplemental Material [29]). Based on this analysis we can conclude that, at $T > \Theta_{CW}$, the SSE is dominated by contributions from short-ranged spin transport. At lower temperatures,

a similar type of analysis could be used to investigate the emerging effects of short-ranged spin correlations in spin transport.

The sign change of the AFM spin Seebeck coefficient, as a function of temperature, below spin flop, at $T^* \approx 0.85T_N$ (Fig. 3) is another feature that is insensitive to $f(T)$, because it is unlikely to change sign in the same region of T . The fact that SBMFT finds T^* lies appreciably to the left of the transition temperature is consistent with a Landau theory for the Néel transition, which has the paramagnetic sign [39]. While a bulk thermal gradient can drive an interfacial spin accumulation with the same sign as Eq. (11) [5], this accumulation may be reduced and possibly invert in sign when umklapp scattering becomes significant. It can reduce the magnon momentum scattering length and occurs when the temperature becomes comparable to the energy of magnons at the Brillouin zone boundary. This occurs for the lower-energy magnon branch before the higher-energy branch, possibly leading to a lower value for T^* . To give a more quantitative estimate for T^* , a bulk spin transport theory for SBs must then be developed.

Acknowledgment. The work was supported by the U.S. Department of Energy, Office of Basic Energy Sciences under Award No. DE-SC0012190.

-
- [1] D. P. Arovas and A. Auerbach, Functional integral theories of low-dimensional quantum Heisenberg models, *Phys. Rev. B* **38**, 316 (1988).
- [2] S.-S. Zhang, E. A. Ghioldi, L. O. Manuel, A. E. Trumper, and C. D. Batista, Schwinger boson theory of ordered magnets, *Phys. Rev. B* **105**, 224404 (2022).
- [3] S. Hoffman, K. Sato, and Y. Tserkovnyak, Landau-Lifshitz theory of the longitudinal spin Seebeck effect, *Phys. Rev. B* **88**, 064408 (2013).
- [4] K. Uchida, T. Kikkawa, A. Miura, J. Shiomi, and E. Saitoh, Quantitative temperature dependence of longitudinal spin Seebeck effect at high temperatures, *Phys. Rev. X* **4**, 041023 (2014).
- [5] S. M. Rezende, R. L. Rodríguez-Suárez, and A. Azevedo, Theory of the spin Seebeck effect in antiferromagnets, *Phys. Rev. B* **93**, 014425 (2016).
- [6] S. Okamoto, Spin injection and spin transport in paramagnetic insulators, *Phys. Rev. B* **93**, 064421 (2016).
- [7] B. Flebus, Y. Tserkovnyak, and G. A. Fiete, Interfacial spin Seebeck effect in noncollinear magnetic systems, *Phys. Rev. B* **99**, 224410 (2019).
- [8] D. Reitz, J. Li, W. Yuan, J. Shi, and Y. Tserkovnyak, Spin Seebeck effect near the antiferromagnetic spin-flop transition, *Phys. Rev. B* **102**, 020408(R) (2020).
- [9] A. Prakash, B. Flebus, J. Brangham, F. Yang, Y. Tserkovnyak, and J. P. Heremans, Evidence for the role of the magnon energy relaxation length in the spin Seebeck effect, *Phys. Rev. B* **97**, 020408(R) (2018).
- [10] S. M. Wu, W. Zhang, A. KC, P. Borisov, J. E. Pearson, J. S. Jiang, D. Lederman, A. Hoffmann, and A. Bhattacharya, Antiferromagnetic spin Seebeck effect, *Phys. Rev. Lett.* **116**, 097204 (2016).
- [11] J. Li, C. B. Wilson, R. Cheng, M. Lohmann, M. Kavand, W. Yuan, M. Aldosary, N. Agladze, P. Wei, M. S. Sherwin, and J. Shi, Spin current from sub-terahertz-generated antiferromagnetic magnons, *Nature (London)* **578**, 70 (2020).
- [12] Y. Shiomi and E. Saitoh, Paramagnetic spin pumping, *Phys. Rev. Lett.* **113**, 266602 (2014).
- [13] S. M. Wu, J. E. Pearson, and A. Bhattacharya, Paramagnetic spin Seebeck effect, *Phys. Rev. Lett.* **114**, 186602 (2015).
- [14] C. Liu, S. M. Wu, J. E. Pearson, J. S. Jiang, N. d'Ambrumenil, and A. Bhattacharya, Probing short-range magnetic order in a geometrically frustrated magnet by means of the spin Seebeck effect, *Phys. Rev. B* **98**, 060415(R) (2018).
- [15] K. Oyanagi, S. Takahashi, L. J. Cornelissen, J. Shan, S. Daimon, T. Kikkawa, G. E. W. Bauer, B. J. van Wees, and E. Saitoh, Spin transport in insulators without exchange stiffness, *Nat. Commun.* **10**, 4740 (2019).
- [16] K. Oyanagi, J. M. Gomez-Perez, X.-P. Zhang, T. Kikkawa, Y. Chen, E. Sagasta, A. Chuvilin, L. E. Hueso, V. N. Golovach, F. S. Bergeret, F. Casanova, and E. Saitoh, Paramagnetic spin Hall magnetoresistance, *Phys. Rev. B* **104**, 134428 (2021).
- [17] K. Oyanagi, S. Takahashi, T. Kikkawa, and E. Saitoh, Mechanism of paramagnetic spin Seebeck effect, *Phys. Rev. B* **107**, 014423 (2023).
- [18] J. Li, Z. Shi, V. H. Ortiz, M. Aldosary, C. Chen, V. Aji, P. Wei, and J. Shi, Spin Seebeck effect from antiferromagnetic magnons and critical spin fluctuations in epitaxial FeF₂ films, *Phys. Rev. Lett.* **122**, 217204 (2019).
- [19] Y. Yamamoto, M. Ichioka, and H. Adachi, Antiferromagnetic spin Seebeck effect across the spin-flop transition: A stochastic Ginzburg-Landau simulation, *Phys. Rev. B* **105**, 104417 (2022).

- [20] S. K. Kim, H. Ochoa, R. Zarzuela, and Y. Tserkovnyak, Realization of the haldane-kane-mele model in a system of localized spins, *Phys. Rev. Lett.* **117**, 227201 (2016).
- [21] R. Samajdar, S. Chatterjee, S. Sachdev, and M. S. Scheurer, Thermal Hall effect in square-lattice spin liquids: A Schwinger boson mean-field study, *Phys. Rev. B* **99**, 165126 (2019).
- [22] E. A. Ghioldi, M. G. Gonzalez, S.-S. Zhang, Y. Kamiya, L. O. Manuel, A. E. Trumper, and C. D. Batista, Dynamical structure factor of the triangular antiferromagnet: Schwinger boson theory beyond mean field, *Phys. Rev. B* **98**, 184403 (2018).
- [23] E. A. Ghioldi, S.-S. Zhang, Y. Kamiya, L. O. Manuel, A. E. Trumper, and C. D. Batista, Evidence of two-spinon bound states in the magnetic spectrum of $\text{Ba}_3\text{CoSb}_2\text{O}_9$, *Phys. Rev. B* **106**, 064418 (2022).
- [24] K. Bolsmann, A. Khudoyberdiev, and G. S. Uhrig, Switching the magnetization in quantum antiferromagnets *PRX Quantum* **4**, 030332 (2023).
- [25] S. Chatterjee and S. Sachdev, Probing excitations in insulators via injection of spin currents, *Phys. Rev. B* **92**, 165113 (2015).
- [26] D. Hirobe, M. Sato, M. Hagihala, Y. Shiomi, T. Masuda, and E. Saitoh, Magnon pairs and spin-nematic correlation in the spin Seebeck effect, *Phys. Rev. Lett.* **123**, 117202 (2019).
- [27] L. Savary and L. Balents, Quantum spin liquids: A review, *Rep. Prog. Phys.* **80**, 016502 (2017).
- [28] L. Messio, C. Lhuillier, and G. Misguich, Time reversal symmetry breaking chiral spin liquids: Projective symmetry group approach of bosonic mean-field theories, *Phys. Rev. B* **87**, 125127 (2013).
- [29] See Supplemental Material at <http://link.aps.org/supplemental/10.1103/PhysRevB.108.L140407> for the additional terms which break $\text{SU}(2)$ symmetry in the most general $\text{U}(1)$ -preserving mean-field decomposition. Since the physical meaning of these terms in the ordered phases is unclear, they are not pursued in the ordered phases of this work.
- [30] B. Flebus, Chemical potential of an antiferromagnetic magnon gas, *Phys. Rev. B* **100**, 064410 (2019).
- [31] O. Tchernyshyov and S. Sondhi, Liquid–gas and other unusual thermal phase transitions in some large- N magnets, *Nucl. Phys. B* **639**, 429 (2002).
- [32] S. Sarker, C. Jayaprakash, H. R. Krishnamurthy, and M. Ma, Bosonic mean-field theory of quantum Heisenberg spin systems: Bose condensation and magnetic order, *Phys. Rev. B* **40**, 5028 (1989).
- [33] E. Erlandsen and A. Sudbø, Schwinger boson study of superconductivity mediated by antiferromagnetic spin fluctuations, *Phys. Rev. B* **102**, 214502 (2020).
- [34] S. Foner, High-field antiferromagnetic resonance in Cr_2O_3 , *Phys. Rev.* **130**, 183 (1963).
- [35] V. S. U. A. Vargas and A. R. Moura, Spin current injection at magnetic insulator/superconductor interfaces, *Phys. Rev. B* **102**, 024412 (2020).
- [36] S. A. Bender and Y. Tserkovnyak, Interfacial spin and heat transfer between metals and magnetic insulators, *Phys. Rev. B* **91**, 140402(R) (2015).
- [37] Y. Luo, C. Liu, H. Saglam, Y. Li, W. Zhang, S. S.-L. Zhang, J. E. Pearson, B. Fisher, T. Zhou, A. Bhattacharya, and A. Hoffmann, Distinguishing antiferromagnetic spin sublattices via the spin Seebeck effect, *Phys. Rev. B* **103**, L020401 (2021).
- [38] Y. J. Kim, C.-Y. Liu, S. K. Lamoreaux, G. Visser, B. Kunkler, A. N. Matlashov, J. C. Long, and T. G. Reddy, New experimental limit on the electric dipole moment of the electron in a paramagnetic insulator, *Phys. Rev. D* **91**, 102004 (2015).
- [39] Y. Yamamoto, M. Ichioka, and H. Adachi, Spin Seebeck effect in paramagnets and antiferromagnets at elevated temperatures, *Phys. Rev. B* **100**, 064419 (2019).